

ITGB2 is a central hub-gene associated with inflammation and early fibro-atheroma development in a swine model of atherosclerosis

Hadjer Namous^a, Maria Giuseppina Strillacci^b, Camila Urbano Braz^a,
Dhanu Shanmuganayagam^a, Christian Krueger^a, Athanasios Peppas^c, William C. Soffregen^d,
Jess Reed^a, Juan F. Granada^{c,*}, Hasan Khatib^{a,**}

^a Department of Animal and Dairy Sciences – University of Wisconsin Madison, WI, USA

^b Department of Medicine Veterinary and Animal Science – University of Milan, Milan, Italy

^c Skirball Center for Innovation, Cardiovascular Research Foundation, New York, NY, USA

^d Northstar Preclinical and Pathology Services, LLC and Skirball Center for Innovation, Cardiovascular Research Foundation, New York, NY, USA

ARTICLE INFO

Keywords:

Atherosclerosis
Gene-expression
Pathways
Hub-genes
Fibro-atheroma

ABSTRACT

Background and aim: The complex dynamic interplay between different biological pathways involved in atherosclerosis development has rendered the identification of specific therapeutic targets a challenging quest. We aimed to identify specific genes and mechanistic pathways associated with the early development of fibro-atheromas in a swine model of atherosclerosis.

Methods: The Wisconsin Miniature Swine™ model of Familial Hypercholesterolemia (WMS-FH, n = 11) and genetically related WMS controls (WMS-N, n = 11) were used. The infrarenal aorta was harvested from both groups for histopathologic and transcriptomic profiling at 12 months. Bioinformatic analysis was performed to identify hub genes and pathways central to disease pathophysiology. The expression of ITGB2, the top ranked hub gene, was manipulated in cell culture and the expression of interconnected genes was tested.

Results: Fibro-atheromatous lesions were documented in all WMS-FH aortic tissues and displayed internal elastic lamina (IEL) disruption, significant reduction of myofibroblast presence and disorganized collagen deposition. No fibro-atheromas were observed in the control group. A total of 266 differentially expressed genes (DEGs) were upregulated in WMS-FH aortic tissues, while 29 genes were downregulated. Top identified hub genes included ITGB2, C1QA, LCP2, SPI1, CSF1R, C5AR1, CTSS, MPEP1, C1QC, and CSF2RB. Overexpression of ITGB2 resulted in elevated expression of other interconnected genes expressed in porcine endothelial cells.

Conclusion: In a swine translational model of atherosclerosis, transcriptomic analysis identified ITGB2 as a central hub gene associated inflammation and early fibroatheroma development making it a potential therapeutic target at this stage of disease.

1. Introduction

Atherosclerosis is a complex disease that changes its structural and biological makeup overtime. Dysfunctional cellular and biological responses within the vessel wall ultimately contribute to the onset and progression of the disease [1–4]. Although significant advances have been made in understanding the pathophysiology of atherosclerosis development, the interplay between different mechanistic pathways is

not fully understood. While advances in atherosclerosis therapeutics continue to grow [5,6], the complex crosstalk between the various pathways involved in disease onset and progression has made the identification of specific therapeutic targets difficult [7–9]. Consequently, targeted treatments to significantly reverse or slow disease progression are limited at the present time. To date, there is still a need to better understand the specific biological pathways involved in the early phases of atherosclerosis development, particularly the role of

* Corresponding author. 1700 Broadway, 9th Floor, New York, NY, 10019, USA.

** Corresponding author. 1675 Observatory Drive, Madison, WI, 53706, USA.

E-mail addresses: namous@wisc.edu (H. Namous), maria.strillacci@unimi.it (M.G. Strillacci), urbanobraz@wisc.edu (C.U. Braz), dshanmug@wisc.edu (D. Shanmuganayagam), ckrueger@wisc.edu (C. Krueger), apeppas@crf.org (A. Peppas), william.c.stoffregen@gmail.com (W.C. Soffregen), jreed@wisc.edu (J. Reed), jgranada@crf.org (J.F. Granada), hkhatib@wisc.edu (H. Khatib).

<https://doi.org/10.1016/j.athplu.2023.11.001>

Received 12 May 2023; Received in revised form 14 September 2023; Accepted 9 November 2023

Available online 15 November 2023

2667-0895/© 2023 The Authors. Published by Elsevier B.V. This is an open access article under the CC BY-NC-ND license (<http://creativecommons.org/licenses/by-nc-nd/4.0/>).

central genes, which may help develop future targeted therapies.

In this study, we aimed to characterize early-stage atherosclerosis transcriptomic signatures and identify key pathways and genes central to the pathophysiology of the disease. We used a swine translational model, the Wisconsin Miniature Swine™ model of Familial Hypercholesterolemia (WMS™-FH), a downsized derivative of the original “Rapacz swine” model [10]. The WMS-FH has a homozygous single-point mutation in the ligand region of the low-density lipoprotein receptor (LDLR) that prevents binding and cholesterol clearance from the blood [10,11] leading to the development of human-like atherosclerotic lesions in different arterial beds starting at 12-months [12–15]. The natural history of disease progression and response to interventional vascular therapies in this animal model has been previously documented [16–19]. A genetically related swine not having the LDLR gene mutation was used as a control (WMS-N). We chose animals that were approximately 12 months old as this age marks a significant transition from pathological intimal thickening to fibro-atheroma development in the lower abdominal aorta in this animal model. We examined specific histopathological features and correlated the gene expression differences between diseased and healthy abdominal aortic tissues aiming to identify novel disease-specific genes and pathways associated with fibroatheroma development.

2. Materials and methods

2.1. Study design and experimental model

The animal protocol was approved by the Institutional Animal Care and Use Committee at the University of Wisconsin-Madison in compliance with the *Guide for the Care and Use for Laboratory Animals* [20] Animal Welfare [21]. Both WMS with (WMS-FH, $n = 11$) and without LDLR mutation (WMS-N, $n = 11$) were randomly selected from the herd and housed at the University of Wisconsin Swine Research and Teaching Center (Madison, WI). All WMS-FH, homozygous for the LDLR mutation, had elevated cholesterol levels, while the WMS control group displayed normal cholesterol profiles. All animals were housed at the same location and consumed a regular diet, formulated with essential nutrients meeting swine feed requirements (Supplemental Table 1). The characteristics of the animals used in the study are summarized in Table 1.

2.2. Tissue collection

Animals at 13.25 ± 0.75 months of age were sacrificed at the University of Wisconsin-Madison Meat Laboratory and Animal Biologics Discovery facility. The abdominal aorta ~2.5 cm above the common iliac artery bifurcation and below the renal arteries was harvested and a 3-cm segment was dissected. This segment was cut into 3 separate 1-cm sections, the center section (segment B) was used for gene expression analyses and the proximal and distal sections (segments A & C, respectively) for histopathology (Fig. 1). The collected segments were flushed with cold Krebs solution to remove blood. The segment allocated to RNA extraction was preserved in RNAlater solution (ThermoFisher Scientific, DE, USA) and stored at -80°C until needed, while the histopathology

Table 1

Characteristics of WMS-FH and normal animal groups: Age, sex, weight, and total cholesterol.

Variable	WMS-FH group	WMS Normal group
Age (months, mean \pm SD)	13.18 (± 0.78)	13.73 (± 0.61)
Females (n, %)	8 (72.72)	6 (54.66)
Males (n, %)	3 (27.28)	5 (45)
Weight* (kg, mean \pm SD)	63.3 (± 13.07)	75.16 (± 8.71)
Total cholesterol** (mg/dL, mean \pm SD)	346.18 (± 74.30)	86.63 (± 19.11)

FH: familial hypercholesterolemia; SD: standard deviation. *: significant difference between groups ($p = 0.021$); **: significant difference between groups ($p = 4.41\text{E-}10$).

segments were placed in 10 % formalin. The infra-renal aortic segment was selected as it is the first to develop fibroatheromas in WMS-FH animals around the selected age of 1 year.

2.3. RNA extraction

Total RNA was extracted from tissues using the RNeasy Mini Kit (QIAGEN, Valencia, CA). Briefly, ≤ 3 mg of the tissue sample from each pig was lyophilized and reduced to powder using liquid nitrogen. Then, pulverized tissues were transferred to a QIAshred column to homogenize and reduce sample viscosity. Subsequent steps followed the manufacturer's instructions. Finally, RNA quality and quantity were assessed using NanodropONE (ThermoFisher Scientific) and Bioanalyzer 2100 Eukaryote Total RNA Nano (Agilent Technologies, CA, USA).

2.4. Histopathology processing

Each animal had two aortic tissue segments except for one WMS-FH animal. A total of 23 WMS-FH and 24 WMS-N aortic segments were submitted for histo-pathological evaluation. Cross-sectional sections (segments A & C) of infrarenal aortic arteries were flushed with Krebs solution. After all the tissue samples were cleared of blood, they were immediately immersed in tubes containing 10 % formalin. The arterial cross-sectional sections were trimmed into proximal and distal segments to create one slice for each segment. The resulting slices were processed and sequentially embedded in paraffin in proximal-distal orientation. Blocks were sectioned twice via microtome, mounted to glass slides and stained with hematoxylin and eosin (H&E) and Elastin Trichrome (ET), with two slides per artery segment. Histopathology analysis was performed by a board-certified veterinary pathologist (WCS). A semi-quantitative scoring system was used to quantify the morphological changes seen in the histological samples.

2.5. RNA-sequencing and differential expression analysis at gene, isoform, and splice variant levels

RNA-Sequencing (RNA-Seq) was performed to assess the differential expression between WMS-FH and WMS-N abdominal aortic tissues. An equivalent amount of RNA from each sample was used to construct three pools per group with 1.5 μg per pool. Supplemental Table 2 summarizes sample distribution across pools and groups. Library preparation and RNA-Seq were performed by LC Sciences (Houston, TX, USA). Upon confirmation of sequencing quality and trimming adapters, obtained reads were mapped to the swine genome (*Sus Scrofa* 10.2) using Bowtie 2 [22]. Transcript abundance at the gene and isoform levels were estimated using RSEM [23]. Differential expression analysis was performed using the “edgeR” R package [24]. To determine differentially expressed splice variants, alternative splicing variant analysis was performed using Multivariate Analysis of Transcript Splicing software for replicates, rMATS [25]. Results were reported for five types of alternative splicing events, including skipped exon (SE), alternative 5' splice site (A5SS), alternative 3' splice site (A3SS), mutually exclusive exons (MXE), and retained intron (RI). Only significant splice variants at a false discovery rate (FDR) ≤ 0.05 were reported.

2.6. Validation of differentially expressed genes (DEGs) with quantitative real-time PCR (qRT-PCR)

Twelve DEGs, found to be significant in the RNA-Seq pools analysis, were selected for validation in individual RNA samples using qRT-PCR. Selection criteria were based on gene function and expression pattern (up/downregulation). Supplemental Table 3 summarizes the selected genes and their corresponding roles in atherosclerosis if known.

Total RNA was extracted from the 22 aortic tissue samples using RNeasy Mini Kit (Qiagen) following the manufacturer's instructions. First, the RNA purity was assessed using NanoDrop™ One (Nanodrop

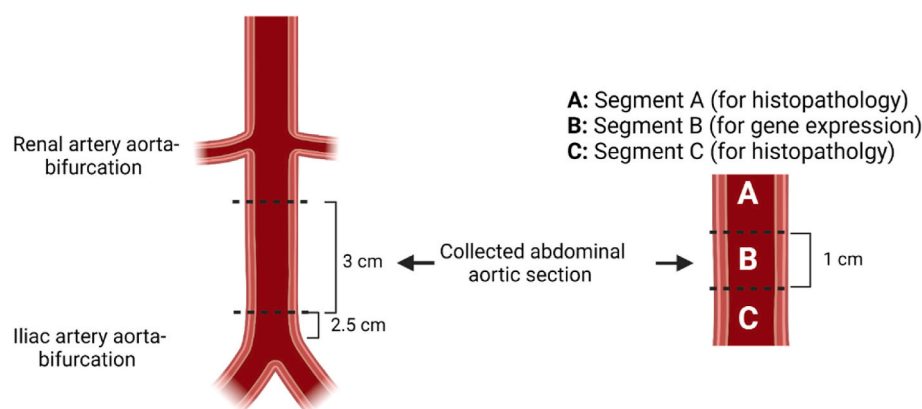


Fig. 1. Schematic describing the abdominal (infrarenal) aortic segments used in the study. **A)** Infrarenal upper segment (1 cm) used to assess histopathology. **B)** Infrarenal middle segment (1 cm) used in gene expression analysis. **C)** infrarenal lower segment also for histopathology assessment. Image made with Biorender (Biorender.com).

Technologies). Next, 100 ng RNA from each sample was used to produce cDNA using the iScript™ cDNA synthesis Kit (BioRad, Hercules, CA). Gene expression was determined for each sample individually by real-time PCR following the iTaq SYBR Green kit protocol (BioRad). Primers were designed to span introns using NCBI primer-blast (<https://www.ncbi.nlm.nih.gov/tools/primer-blast/>) (Supplemental Table 4). The YWHAZ gene was selected as a reference control for its stability across all samples. The relative gene expression was evaluated using the $2^{-\Delta\Delta CT}$ method [26].

2.7. Protein-protein interaction network, pathway enrichment, and hub gene analyses

To identify protein-protein interactions between DEGs, we selected genes with significant differential expression at $FDR \leq 5\%$. To construct a protein-protein interaction (PPI) network, the Search Tool for the Retrieval of Interacting Genes/Proteins (STRINGdb v10.5) [27] was used. The medium confidence score of the PPI network was set to 0.4. To determine the biological function and relation in which the protein products of DEGs are involved, we performed gene ontology (GO) of biological processes (BP) and Kyoto Encyclopedia of Genes and Genomes (KEGG) pathway enrichment analyses using ClueGO [28] in Cytoscape. ClueGO kappa score ($\kappa > 0.4$) was used to define term-term interrelation and functional groups based on shared genes between terms. Hence, BP and KEGG terms/pathway results were grouped under the most significant term. Similar analysis was carried out for differentially expressed isoforms. Determining hub genes within a PPI network allows for identifying central genes to the pathophysiology of the disease and potential therapeutic targets. We used the Cytohubba plug-in [29] in Cytoscape to identify the hub genes. Genes were scored using the Maximal Clique Centrality (MCC) method, and the 10 highest-scoring genes were reported.

2.8. ITGB2 gRNA sequences design and plasmid constructs

The integrin subunit $\beta 2$ (*ITGB2*) is at the center of most interconnections with other genes within the PPI network; hence, it was selected for expression manipulation via epigenome editing. *ITGB2* promoter-specific guide RNA (gRNA) sequences were designed with CRISPOR [30]; *ITGB2* gRNA1: 5'TCATACAGTCCGTCTTG3' and *ITGB2* gRNA2: 5'TGTGCCTGTGTCACGCCCGG 3'. The gRNAs spanned a 494 bp region upstream of the *ITGB2* gene. The gRNAs oligonucleotides were synthesized by Integrated DNA Technologies (IDT Technologies, IA, USA). *ITGB2* gRNA expression plasmids were constructed by ligating annealed gRNA oligonucleotides using T4 ligase (NEB, USA) to psPgRNA vector (Addgene, cat# 47,108). The dCas9-p300 plasmid construct was

obtained from Addgene (cat#61357).

2.9. Cell culture of porcine aortic endothelial cells and manipulation of ITGB2 expression

ITGB2 was the top hub gene with multiple interactions within the PPI network. The high interconnectivity of *ITGB2* with other genes suggests its participation in multiple pathways, making it a promising therapeutic target. To assess the impact of *ITGB2* expression on inter-connected genes in a manner consistent with differential expression and PPI network analyses, we decided to overexpress *ITGB2* in porcine aorta endothelial cells (PAECs) obtained from iXCells Biotechnologies (CA, USA). Cells were grown in iXCells Biotechnologies' Endothelial Cell Medium supplemented with Basal medium and Endothelial Cell Growth Supplement (ECGS). Cells were incubated at 37 °C in humidified 5 % (v/v) CO₂-containing atmosphere.

For the overexpression of *ITGB2*, PAEC cells were transfected with dCas9-P300 and *ITGB2* gRNAs constructs between the third and seventh passages. Cells were seeded in 6-well plates (1 well per treatment/control), and 24 h after seeding, they were transfected with lipofectamine 2000 (Life Technologies), 2.25 μ g of dCas9-p300, and 0.75 μ g of an equimolar concentration of each *ITGB2* gRNA expression vector. Two days post-transfection, cells were harvested, and RNA was extracted using Direct-zol RNA MiniPrep Kit (Zymo Research, CA, USA) following manufacturer's instructions. All transfections were performed in three biological replicates. *ITGB2* overexpression was assessed via qRT-PCR, and fold change expression between transfected and nontransfected cells was determined using the $2^{-\Delta\Delta CT}$ method. Genes from the PPI network connected directly (*C3* and *FCER1G*) or indirectly (*S100A4* and *CD68*) with *ITGB2* were selected to assess their expression. The other evaluated genes (*MMP9*, *LCP1*, *ACTC1*, and *CNN1*) demonstrated no expression in either control or treated cells.

2.10. Statistical analysis

The statistical significance of DEGs was determined using a binomial linear regression model coupled with multiple testing adjustment inherent in the edgeR package. For gene expression validation via qRT-PCR, a two-tail *t*-test was used to determine the statistical significance of relative gene expression (ΔCT values) between WMS-FH and WMS-N samples. To determine sex differences in gene expression, we performed a linear regression model with sex, weight and group (WMS-FH vs WMS-N) variables using ΔCT values from qRT-PCR data. The statistical significance of gene expression in the cell culture experiments was assessed using paired *t*-test. Statistical significance was determined when the *p*-value was < 0.1 .

3. Results

3.1. Atherosclerosis stage and disease phenotype

Intimal hyperplasia was observed in 17 of 23 (74 %) of the WMS-N arteries and 17 of 24 (71 %) of the WMS-FH arteries (Supplemental Table 5). The severity of intimal hyperplasia was higher in the WMS-FH (mean score = 1.38 ± 0.24 ; mean percentage of circumference involved = 28.1 ± 4.3 %) compared to the WMS-N mean score = 0.74 ± 0.09 ; mean percentage of circumference involved = 17.6 ± 3.2 %). Pathological changes consistent with atheromatous changes were seen in all of the WMS-FH arterial segments and none in the WMS-N control group (Fig. 2).

The pathological neointima of the WMS-FH arteries was composed of connective tissue including low density myofibroblasts and exhibited variable levels of lipid (17/17, 100 %), macrophage infiltration (17/17, 100 %), cholesterol clefts (11/17, 65 %), and mineralization (3/17, 18 %). Macrophages infiltration was mainly observed in WMS-FH. While no specific staining was used to determine the type of infiltrating macrophages, our RNA sequencing data shows an upregulation of both M1 and M2 type macrophages markers in WMS-FH atheromatous tissues including: CD68, CD86, and CD32 for M1 macrophages; CLEC7A, CSF1R, and PPARG for M2 macrophages (Supplementary Table 6). Overall, there was more than 50 % reduction of myofibroblast presence in the WMS-FH compared to the control group. However, collagen was more abundant but organized differently in the WMS-FH compared to the WMS-N control group. In the WMS-FH arteries, foci of dense collagen unassociated with myofibroblasts were seen in each affected arterial segment, whereas collagen was evenly interspersed between the myofibroblast cells in the WMS-N control group. Vacuolation consistent with lipid infiltration was observed in the tunica media of 12 of 24 (50 %) WMS-FH arteries and 0 of 23 (0 %) WMS-N arteries. The medial lipid was always subjacent to the segmental region of intimal hyperplasia, exhibiting the atheromatous changes in the affected WMS-FH arteries (Fig. 3).

Histological alterations consistent with underlying arterial wall

injury were more commonly observed in the WMS-FH group and included disruption of the internal elastic lamina (IEL) (WMS-FH = 12 of 24, 50 %; WMS-N = 6 of 23, 26 %) and adventitial fibrosis (WMS-FH = 14 of 24, 58 %; WMS-N = 19 of 23, 83 %). When present, the disruption/loss of the IEL was in small focal or multifocal areas subjacent to the intimal hyperplasia.

3.2. Identification of DEGs

A total of 22 abdominal aortic tissue samples from WMS-FH (n = 11) and WMS-N (n = 11) swine were used in this analysis. RNA extracted from all samples was pooled (n = 3 pools per group) and sequenced. RNA-Seq analysis revealed 295 DEGs between the two groups at 5 % FDR. In the WMS-FH group, 266 genes were upregulated and the remaining 29 DEGs were downregulated (Fig. 4 B and C, Supplemental Table 6). Similarly, 186 isoforms were differentially expressed (DEIs) at 5 % FDR, with 169 upregulated isoforms and 17 downregulated isoforms (Fig. 4 A and C; Supplemental Table 7). In addition to gene- and isoform-level differential expression, 13 splice variants were captured. These variants belonged to 9 DEGs (Supplemental Table 8).

3.3. Validation of DEGs via qRT-PCR

The present work used a pooling strategy for RNA sequencing to determine DEGs between WMS-FH and WMS-N groups. Hence, we selected 12 DEGs for validation in the individual samples used to construct the pools (Supplemental Figure 2). Differential gene expression results of the mRNA sequencing showed high expression of the *CXCL14*, *APOE*, *LCP1*, *ITGB2*, *AIF1*, *CD36*, *TLR4*, and *TLR6* genes in WMS-FH pools compared to the WMS-N control pools. Similarly, the relative gene expression analysis in individual samples showed significantly higher expression of these genes in WMS-FH compared to WMS-N samples with a fold change (FC) of 11.83 for *CXCL14* ($p = 0.010$), 9.70 for *APOE* ($P = 0.005$), 5.01 for *LCP1* ($p = 0.028$), 3.75 for *ITGB2* ($p = 0.010$), and 2.84 for *AIF1* ($P = 0.031$). *CD36* showed high expression in WMS-FH; however, no significant differences were observed ($FC = 2.00$,

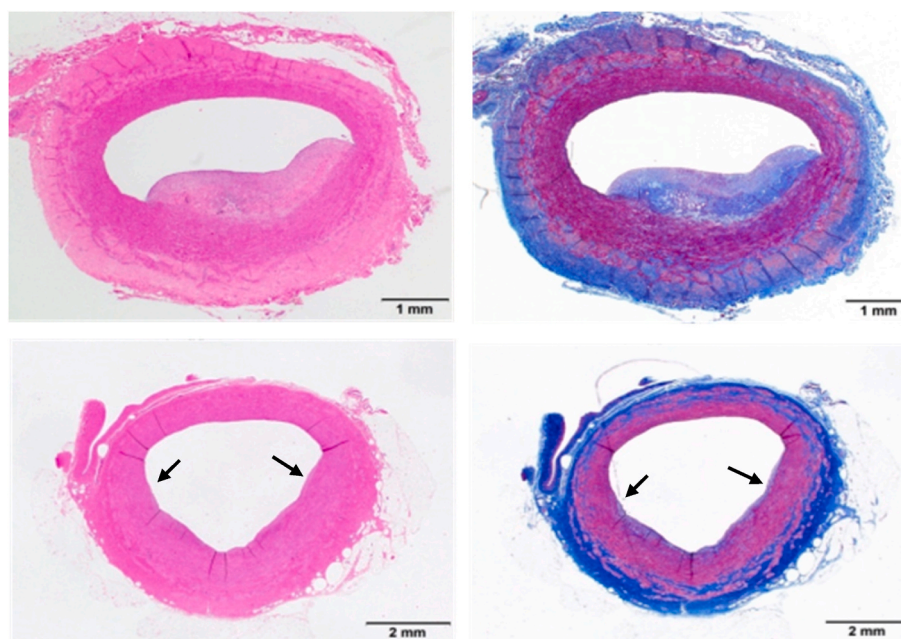


Fig. 2. Histopathology of representative animals from WMS-FH and WMS-N. Photograph is the top row includes representative histopathology images (H&E left, ET right) of an aortic section of the WMS-FH group. There is a segmental area of intimal hyperplasia consistent with atheromatous change. Lipid and cholesterol clefts are contained within the neointima that also contains a large area of dense collagen with small numbers of myofibroblasts. The lower panels are representative pictures of the aorta in the control WMS group are shown. Segmental region of slight intimal hyperplasia composed of myofibroblasts and associated connective tissue matrix, mostly collagen are shown.

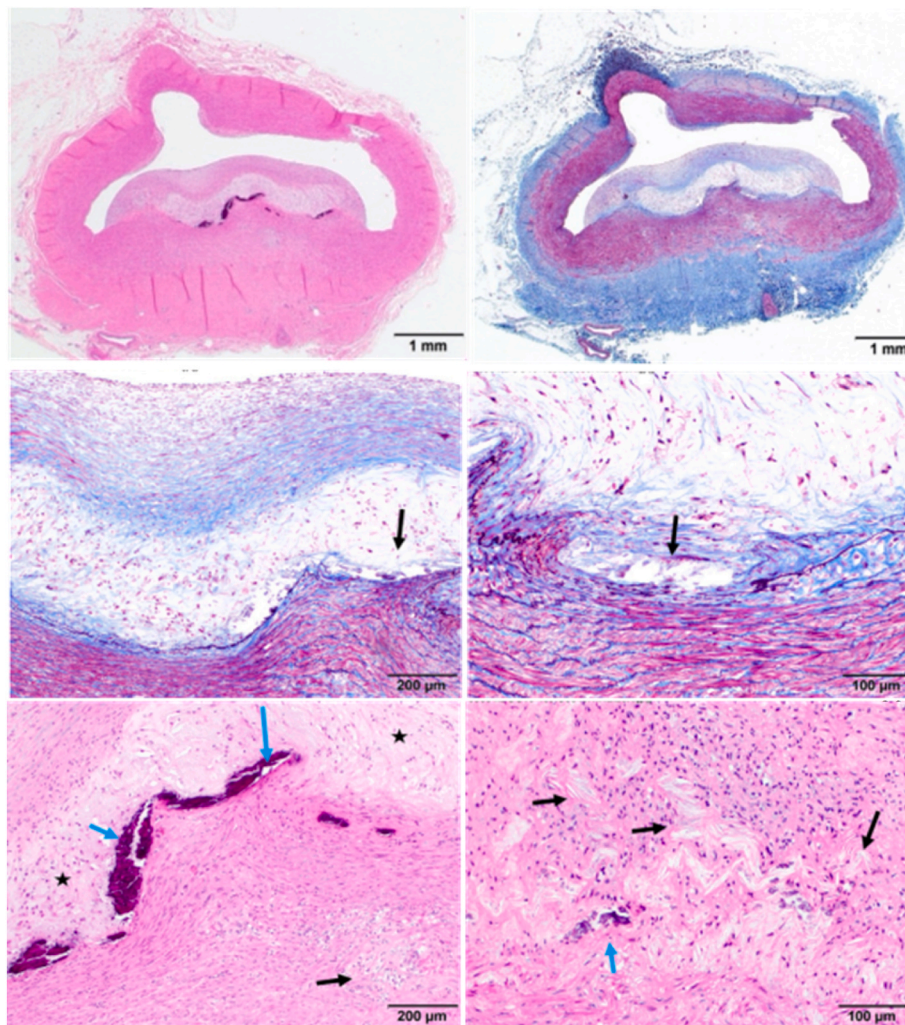


Fig. 3. Intimal thickening to the early phases of fibro-atheroma formation in WMS-FH. Photographs in the top row (left HE, right ET) are representative pictures of the aorta in the WMS-FH group in which there is a segmental area of intimal hyperplasia consistent with atheromatous changes as well. Clefts of mineralization at the interface of the neointima and IEL. There is additionally a central core of lipid, and an outer region of collagen with small numbers of myofibroblasts. Mid panel displays the interface of the lipid-rich neointima and the tunica media (left:10 \times ; right: 20 \times). There are small disruptions of the IEL (arrows). Bottom left panel presents the neointima, which contains a large region of lipid (stars), and the inner media which contains foci of vacuolation/lipid infiltration (black arrow). There are clefts of mineralization at the interface of the neointimal and media (blue arrow). The bottom right panel shows the neointima which contains lipid and cholesterol clefts (black arrows) among collagen and occasional foci of mineralization (blue arrow). (For interpretation of the references to color in this figure legend, the reader is referred to the Web version of this article.)

$p = 0.157$). Similar to RNA-Seq results, relative gene expression for the *TLR4* confirmed the differential expression with an FC = 3.51 ($p = 0.029$). In contrast, *TLR6* showed a lower expression in WMS-FH (FC = 0.36, $p = 0.012$).

CYP2B22, *CILP2*, *CNN1*, and *ACTC1* genes were downregulated in WMS-FH pools compared with WMS-N pools. For this set of genes, only *CYP2B22* and *CILP2* showed a significant relative gene expression between the groups, thus validating the sequencing results. Fold change differences were 16.3 for *CYP2B22* ($p = 0.009$) and 3.79 for *CILP2* ($p = 0.034$). *CYP2B22* showed an almost exclusive expression in the WMS-N group. *CNN1* (FC = 0.81) and *ACTC1* (FC = 0.40) showed no significant differences in relative gene expression between the two groups.

We also assessed sex differences in expression of tested genes. Significant differential expression levels between females and males within both groups were found for *CXCL14* ($p = 0.009$), and *CYP2B22* ($p = 0.031$) genes only. Other tested genes showed no significant differences between sexes (Supplemental Table 9).

3.4. Functional enrichment and hub gene analyses

We carried out a PPI network analysis to predict interactions between the DEGs and identify the involved mechanisms. The constructed PPI network was significantly enriched ($p < 1.0e-16$) for interactions between the DEGs, indicating that the proteins are biologically connected (Supplemental Figure 1). Additionally, we performed a pathway enrichment analysis focused on biological processes (BP) and KEGG pathways. Gene ontology of BP analysis suggests that the DEGs primarily function in the immune system and inflammatory responses. Specifically, the regulation of the immune system process was the most enriched BP, followed by phagocytosis, inflammatory response, myeloid cell differentiation, and leukocyte activation. Other significant BPs are listed in Supplemental Figure 3 B and Supplemental Table 10.

KEGG pathway enrichment analysis showed that DEGs are enriched in the phagosome, *staphylococcus aureus* infection, Fc epsilon RI signaling, osteoclast differentiation, lysosome, malaria, cholesterol metabolism, leukocyte transendothelial migration, natural killer cells mediated toxicity, chemokine signaling, and PPAR signaling pathways

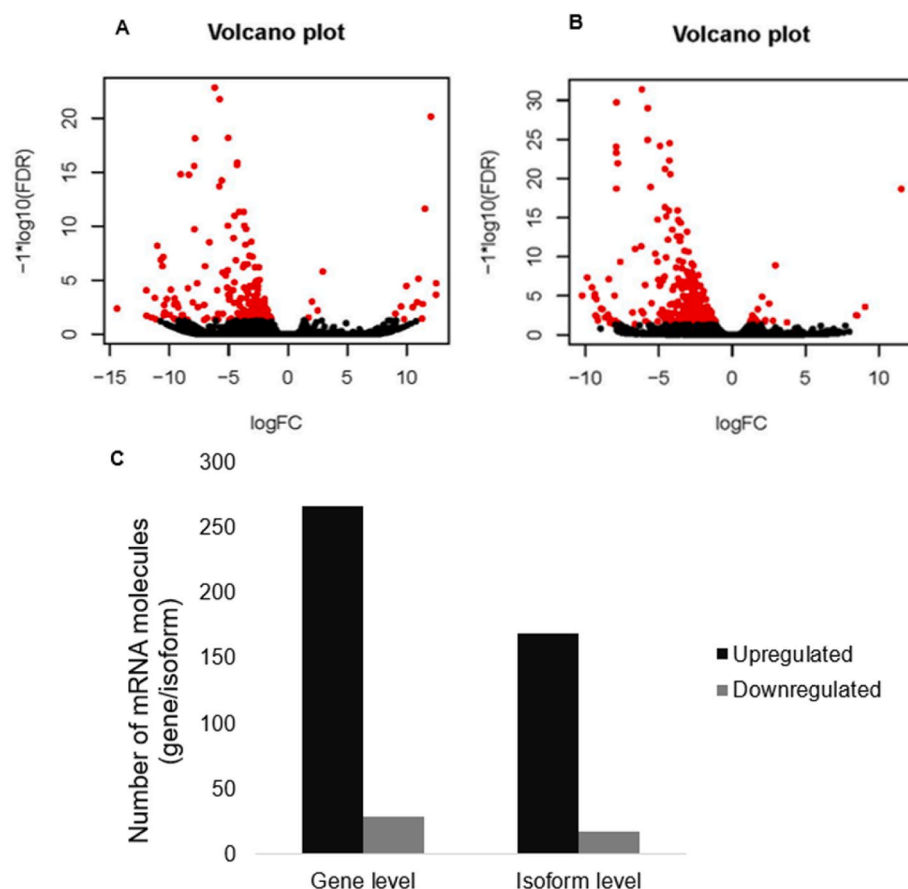


Fig. 4. Differential expression between WMS-FH and WMS-N at gene and isoform levels. **A)** Volcano plot for isoform-level differences. **B)** Volcano plot for gene-level differences. A negative $\log_{2}(\text{FC})$ indicates upregulation in WMS-FH. **C)** Number of differentially expressed genes and isoforms between abdominal aortic tissues from WMS-FH and WMS normal (5 % FDR).

(Supplemental Figure 3 A, Supplemental Table 11). Similar findings were obtained for differentially expressed isoforms where BPs and KEGGs involved in inflammation, immune responses, and cholesterol metabolism were enriched (Supplemental Tables 12 and 13).

Given the complexity of networks and the crosstalk between pathways, we analyzed the PPI for hub genes. Hub genes have high interconnectivity levels and central roles in the PPI network and could become potential therapeutic targets. The 10 highest scored and most significant nodes within the PPI network were selected as hub genes (Table 2). Our findings indicate that *ITGB2*, *C1QA*, *LCP2*, *SPI1*, *CSF1R*, *CSF2RB*, *C5AR1*, *CTSS*, *MPEG1*, and *C1QC* genes (Fig. 5) are the most central to the pathophysiology within the DEGs obtained. The hub genes participate in a variety of pathways and biological pathways (Fig. 6) with the mostly enriched one being the complement and coagulation cascades ($p = 1.3 \times 10^{-6}$) in which *C1QA*, *C1QC*, *C5AR1*, and *ITGB2* genes are involved.

3.5. *ITGB2* upregulation in PAECs and its effect on interconnecting genes

The goal of this experiment was to investigate the effect of over-expressing one gene (central hub gene) on the expression of other genes, regardless of the cell type. *ITGB2* was the top hub gene with the highest interconnections with other genes within the PPI network. Hence it is at the core of interactions and enriched pathways. Indeed, our analysis showed that *ITGB2* participates in many KEGG pathways and has interconnections with other DEGs also enriched in the reported KEGG pathways (Fig. 6). Therefore, manipulating the expression of *ITGB2* would likely affect the expression of the interconnected genes.

Transfection of PAECs with dCas9-p300, which adds acetyl groups to

the *ITGB2* promoter region, resulted in a 3.13-fold change expression ($p = 0.032$) of *ITGB2*. Consequently, we measured the expression of *C3*, *FCER1G*, *S100A4*, and *CD68*, which were selected based on their interconnectivity with *ITGB2* within the PPI network (Fig. 7). Upon over-expression of *ITGB2*, the expression of *C3*, *CD68*, *S100A4*, and *FCER1G* was increased by 2.36 ($p = 0.063$), 2.75 ($p = 0.001$), 1.61 ($p = 0.076$), and 1.67 ($p = 0.017$) fold changes, respectively (Fig. 8). Other tested genes were not expressed in PAECs before or after *ITGB2* expression manipulation.

4. Discussion

Atherosclerosis is a chronic disease that develops over several decades and whose pathobiological mechanisms change according to its stage of development. In this study, we aimed to investigate the transcriptomic profile and biological mechanisms involved in the early stages of atherosclerosis development using a large translational model of the disease (WMS-FH) and a genetically related control group (WMS-N). We confirmed the presence of atherosclerosis using histology and correlated the microscopic pathology with the transcriptomic findings.

The main findings of our study are; a) fibroatheromas in the distal abdominal aorta were found in all WMS-FH but not in the WMS-N controls, b) a reduction in myofibroblast presence and increase in disorganized collagen deposition were prominent histological features in WMS-FH lesions, c) PPI network analysis identified 10 hub genes primarily involved in cellular inflammatory pathways and e) *ITGB2* was the central hub gene presenting the highest number of interconnections with other genes within the PPI network and is involved in multiple pathways.

Table 2
Top 10 hub genes within protein-protein interaction network ranked using Cytohubba - MCC method.

Rank	Gene	Description	MCC Score	Protein	Protein Function	Reported role in Atherosclerosis
1	ITGB2 ^{a,b}	Integrin Subunit Beta 2	1.0810 E+08	CD18	Cellular adhesion to ECM and surface signaling	Monocyte trafficking to the subendothelium (40,62).
7	C5AR1 ^{a,b}	Complement C5a Receptor 1	9.8356 E+07	CD88	G-protein-coupled receptor for C5a	Participates in inflammation via binding to proinflammatory C5A (64)
2	C1QA ^b	Complement C1q A Chain	1.0808 E+08	Complement C1q subcomponent subunit A ³	Subunit A of the 1st component of the serum complement system (C1Q)	C1Q regulated leukocyte recruitment (68).
10	C1QC ^b	Complement C1q C chain	9.5626 E+07	Complement C1q subcomponent subunit C	Subunit C of the 1st component of the serum complement system (C1Q)	Classical complement cascade pathway promotes inflammation aggravating atherosclerosis in advanced lesions (67).
3	LCP2	Lymphocyte Cytosolic Protein 2	1.0798 E+08	SLP-76	Signal-transducing adaptor protein	Role in atherosclerosis is yet to be described.
4	SPI1 ^c	Hematopoietic Transcription Factor PU.1	1.0793 E+08	SPI1 proto-oncogene	ETS-domain transcription factor that activates gene expression during myeloid and B-lymphoid cell development	Myeloid cell differentiation (75). Exact role in atherosclerosis is yet to be described.
5	CSF1R ^c	Colony Stimulating Factor 1 Receptor	1.0732 E+08	Receptor for colony stimulating factor 1	Controls the production, differentiation, and function of macrophages	Participate in atherosclerosis progression by regulating macrophages proliferation, differentiation and migration to lesion (72–74)
6	CSF2RB ^c	Colony Stimulating Factor 2 Receptor Subunit Beta	1.0603 E+08	Common beta chain of the high affinity receptor for IL-3, IL-5 and CSF	Controls the production, differentiation, and function of macrophages	
9	MPEG1	Macrophage Expressed 1	9.6209 E+07	protein belonging to the Membrane Attack Complex/Perforin (MACPF)	pore-forming protein expressed in macrophages and neutrophils	
8	CTSS	Cathepsin	9.6714 E+07	Cathepsin S	Secreted cathepsin S cleaves some extracellular matrix (ECM) proteins. Cathepsin S may be considered the most potent elastase known.	Participates in progression of atherosclerosis by mediating macrophages phagocytosis (76). Degrades collagen in lesions (51).

^a Leukocyte trafficking and *trans*-endothelial migration.
^b The complement cascade.
^c Macrophage proliferation and differentiation.

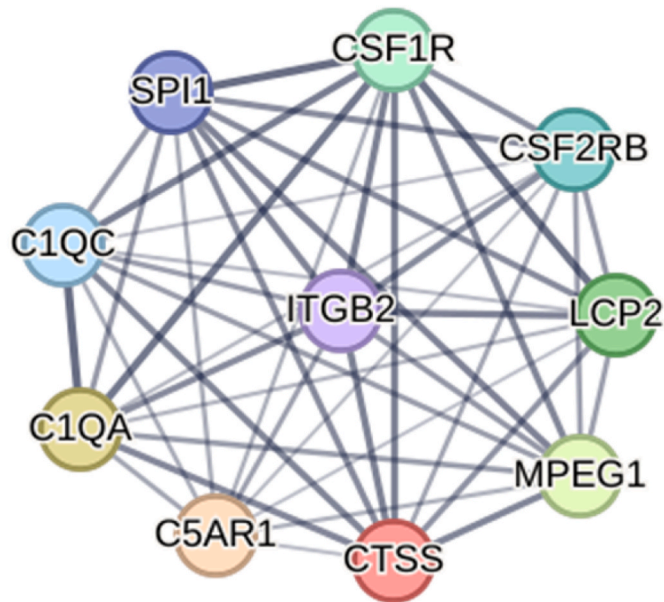


Fig. 5. Hub genes within the Protein-Protein interaction network. Node represents the genes with their respective names. Edges connecting nodes represent evidence of interaction between two genes.

4.1. Swine model and atherosclerosis phenotype

The WMS-FH is a well-characterized model of atherosclerosis [17, 31–33], offering a unique opportunity to study the biological mechanisms involved in disease development in a controlled environment. Previous histological studies have shown that early atheromatous lesions start to be identifiable by 12 months at the distal abdominal aorta,

then we selected this time-point as this marks the initiation of fibroatheroma development in this model. Histopathology confirmed the presence of fibroatheromas in all arteries in the WMS-FH group and no evidence of the disease in the WMS-N control group. The phenotype of these lesions represents the transition phase into the early phases of fibro-atheroma formation, a critical stage in which disease progression could be modified by targeting specific biological pathways. A striking pathological feature was the reduced presence of myofibroblasts, and the disorganized presence of collagen deposition within the neointima. Organized collagen deposition is essential for the stability of fully developed atheromas [34,35], and plaque rupture and instability have been associated with collagen loss, a histological landmark of thin cap fibroatheromas [36]. Our findings confirm that changes in myofibroblast content and abnormalities in collagen deposition play an important role in the early phases of atherosclerosis development.

4.2. Transcriptomic profile and relevance to human atherosclerosis

In our study, RNA-Seq data demonstrated a distinct gene expression pattern between the diseased WMS-FH and normal WMS-N control group, including expression differences at isoform levels. Our results showed that several DEGs correlated with the pathology results further confirming the observed changes in gene expression in data already published in human studies of atherosclerosis transcriptome [37–39]. Macrophages infiltration and foam cells formation, one of the hallmarks of atherosclerosis, were consistently seen in all histological samples of the WMS-FH. These findings correlate with leukocyte trans-endothelial migration, chemokine signaling pathways, phagosome and lysosome pathways enriched in our analysis. These pathways are known to be involved from the early phases of atherosclerosis development [40, 41]. DEGs participating in these pathways are upregulated in WMS-FH further confirming that they are active in these animals during the early stage of the disease. Furthermore, the observed upregulation of DEGs active in the peroxisome proliferator-activated receptor (PPARs)

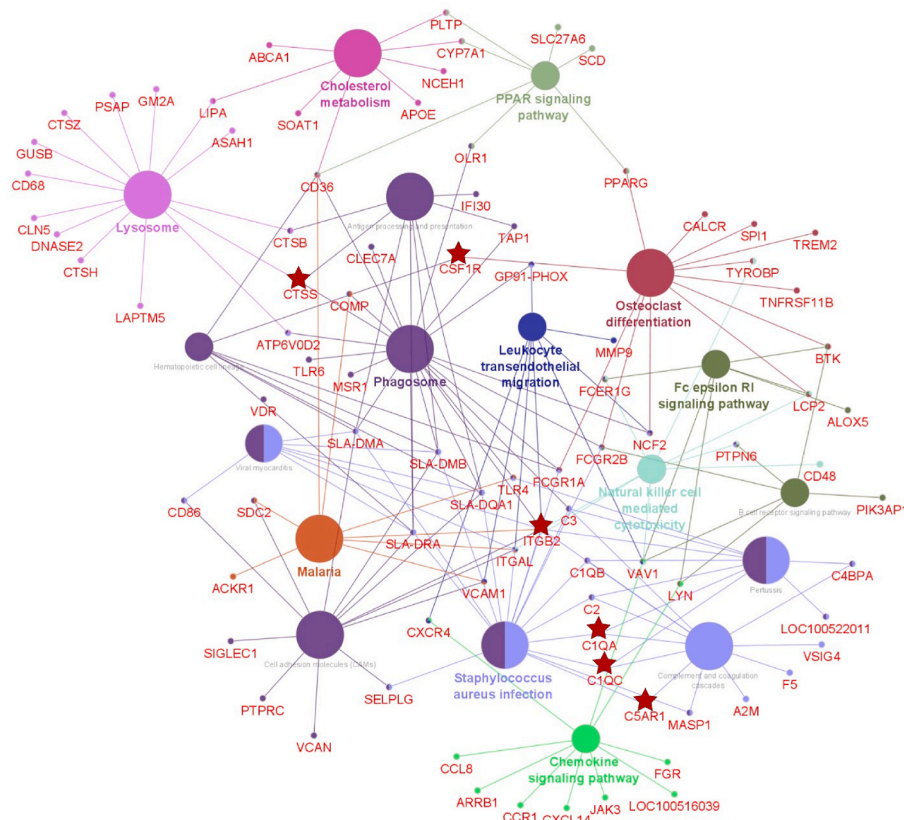


Fig. 6. Enriched KEGG pathways and participating differentially expressed genes. Edges correspond to interactions between DEGs, pathways, and DEGs and pathways. Pathways with the same color are related. Hub genes are indicated with a red star. (For interpretation of the references to color in this figure legend, the reader is referred to the Web version of this article.)

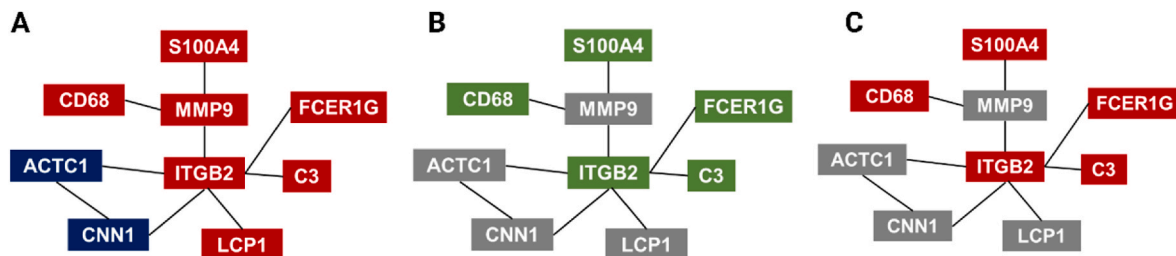


Fig. 7. Interaction networks for ITGB2 and tested genes with color coding for expression patterns in WMS-FH. **A)** Differentially expressed genes from RNA sequencing data (red and blue indicate upregulation and downregulation of gene expression in WMS-FH animals, respectively.). **B)** Expression pattern of the same genes in nontreated porcine aortic endothelial cells (Green indicates expression of gene whereas gray indicates no expression). **C)** Changes in expression of genes in treated porcine aortic endothelial cells overexpressing ITGB2 (Red indicates increased expression of gene; gray indicate no expression). (For interpretation of the references to color in this figure legend, the reader is referred to the Web version of this article.)

signaling pathway is likely an adaptation to clear cholesterol from tissue and promote macrophage cholesterol efflux. Similar pathways were also reported in human studies of atherosclerosis transcriptome [37–39].

Multiple vessel wall abnormalities including a reduction in the number of myofibroblasts, rupture of the IEL, increase in collagen deposition and presence of micro calcification were seen in the WMS-FH group. Lipid uptake induces a shift in vascular smooth muscle cells (VSMCs) phenotype to a macrophage/foam-like proinflammatory phenotype [42,43] inducing the production of large amounts of extracellular matrix (ECM) proteins such as collagen and metalloproteinases (i.e., MMP9 upregulated in WMS-FH, Supplemental Table 6) [44,45]. Chinetti-Gbaguidi et al. [46] showed that macrophages in lesions exhibit osteoclast-like function, which suggests that mechanisms of calcification resorption are in place in WMS-FH. In our study, the osteoclast differentiation pathway was upregulated in WMS-FH. Finally, the

progressive loss of the elastic fibers in the internal lamina suggests an aberrant ability to restore the elastic tissue. Also, increased IEL disruption may trigger cellular proliferation, altering collagen production [47]. Subsequently, microscopic mineralization/calcification occurs [48], which was observed in the arteries of our WMS-FH.

The WMS-FH histopathology showed a distinct pattern of collagen distribution in the neointima compared to WMS-N, showing foci of dense collagen not associated with myofibroblasts in each atherosclerotic lesion. Myofibroblasts are essential for maintaining the structural integrity of tissue via the secretion of elastin and collagen [49]. The reduction and uneven distribution of collagen in WMS-FH suggests a decrease in either its production or degradation. Indeed, our findings showed an increased expression of MMP9, MMP19, and CTSS in WMS-FH (Supplemental Table 6). These genes are known to degrade ECM proteins including elastin and collagen [50,51]. Furthermore,

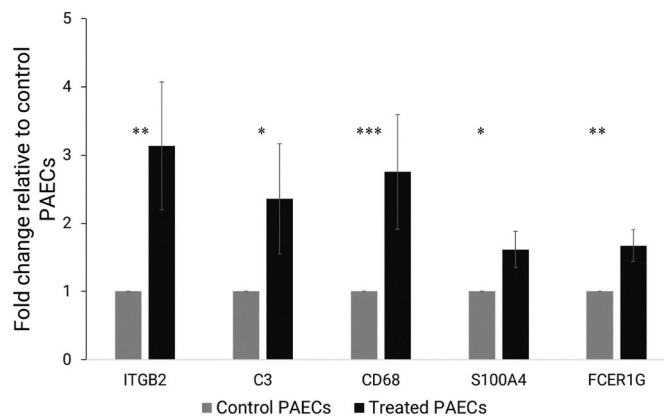


Fig. 8. Relative gene expression of ITGB2, C3, FCER1G, S100A4, and CD68 in non-treated and treated PAECs. Treated PAECs overexpress ITGB2. Fold change was calculated using $2^{-(\Delta\Delta CT)}$ of treated PAECs – Δ of control PAECs. Data in the Figure represent three biological replicates. Error bars represent the standard deviation in fold change difference. ***: $p < 0.01$, **: $p < 0.05$, *: $p < 0.1$.

CNN1, ACTA1, ACTC1, CSRP1, COMP, and DES were found to be downregulated in WMS-FH (Supplemental Table 6). These genes are associated with healthy VSMCs phenotype and participate in muscle contraction and actinin binding, and the observed downregulation indicates a change in VSMC phenotype and altered function. Altered functions of VSMCs in the medial layer include vascular calcification and formation of the fibrous cap covering the plaques [52]. Recently, human studies have shown that VSMCs expand to different cells present in atherosclerosis lesions [53–55]. Furthermore, a sign of expanding VSMCs is the upregulation of Complement C3, which is highly upregulated in WMS-FH (Supplemental Table 6), and its effect on macrophages and VSMCs proliferation [53]. These studies further confirm the aberrant phenotype VSMCs are exhibiting within WMS-FH arteries and the observed distribution and amount of myofibroblasts and collagen.

4.3. Hub genes and early atherosclerosis development

As many DEGs are shared between biological pathways, selecting core genes from the constructed PPI network is the likeliest approach to identifying those with the highest therapeutic potential. In the present work, we identified 10 hub genes central to the pathogenesis of atherosclerosis. These identified hub genes exhibited upregulation in WMS-FH atherosclerotic aortic tissues and included ITGB2, C1QA, LCP2, SPI1, CSF1R, C5AR1, CTSS, MPEG1, C1QC, and CSF2RB. Of the hub genes identified, ITGB2 [39,56–60], C1QA [61], C1QC [58,61], CSF1R [57,61], C5AR1 [57], and CTSS [39] have been reported as hub genes associated with atherosclerosis development in human studies. Additionally, the genes functions have been associated with early disease development through modulation of various mechanisms including leukocyte trafficking and transendothelial migration, macrophages proliferation and the complement cascade.

4.3.1. Leukocyte trafficking and trans-endothelial migration

ITGB2 is commonly known to be expressed on monocyte surfaces that binds adhesion molecules on endothelial cells upon endothelial dysfunction and participate in monocyte trafficking to the sub-endothelium [4,40,62]. Similarly, C5AR1 is a receptor for the pro-inflammatory C5A and it has been associated with leukocyte recruitment to sites of inflammation [63]. Niyonzima et al. [64] showed that C5AR1 mediates signaling to control IL-1 β production, altering mitochondrial activity, and increasing reactive oxygen species production. Additionally, the authors showed that the deletion of C5AR1 in myeloid cells in mice reduced the severity of atherosclerosis [64]. Given that ITGB2 (CD18) was the top-ranked hub gene, we opted to assess the

effect of manipulating its expression on interacting genes to validate the observed expression pattern in RNA-Seq data. In this analysis, overexpression of ITGB2 in PAECs increased the expression of the tested interconnecting genes making this gene a potential therapeutic target at the early stages of atherosclerosis. Previous studies in mice demonstrated that depletion or inhibition of ITGB2 reduced lesion sizes and monocyte trafficking [40,65]. Thus, our results suggest a potential therapeutic effect of this hub gene.

4.3.2. The complement cascade and atherosclerosis progression

ITGB2 and C5AR1 are also enriched in the complement cascade pathway along with C1QC, and C1QA. C1QC and C1QA are sub-components of C1Q, the first protein in the classical complement pathway. C1Q has been shown to modulate the uptake of atherogenic lipoproteins [66] and also have a proinflammatory effect that can accelerate the development of atherosclerosis [67]. Moreover, C1Q regulates collagen-induced platelet activation, reactive oxygen species (ROS) production, and associated leukocyte recruitment during vessel wall injury [68]. A recent study in humans also showed increased expression of C1Q in abdominal and coronary aortas with atherosclerosis [69]. Additionally, ITGB2 constitutes the clearance receptor that binds the cleaved product of complement 3 (C3) a major protein in the complement cascade [70]. Complement activation generates proinflammatory mediators which in turn activate the endothelium and enhance leukocyte recruitment to sites of inflammation. A study in mice demonstrated that atherosclerosis progression from foam cells to advanced lesions depends on the presence of an intact activated complement system [71]. Hence, these upregulated hub genes in WMS-FH suggest that activation of the complement pathway plays an important role in the early phases of atherosclerosis development.

4.3.3. Macrophage proliferation and differentiation

Hub genes CSF1R, CSF2RB, and MPEG1 have been associated with atherosclerosis progression by regulating macrophage proliferation, differentiation [72], and migration into the lesions [73,74]. SPI1 is upregulated during myeloid cell differentiation [75] which is consistent with our observation of the significant increase in SPI1 expression in WMS-FH, further suggesting that the activation of myeloid cells and differentiation into macrophages contributes to atherosclerosis progression. Additionally, macrophages in lesions activates phagocytosis in an attempt to clear oxLDL from the lesion. CTSS has been shown to mediate phagocytosis [76] and collagen degradation [51] during atherosclerosis development.

Based on the transcriptomic and pathology correlation results, our findings suggest that ITGB2 plays a central role within the other top hub genes and it is associated with inflammation and the development of atherosclerosis by affecting key cellular-mediated pathways such as leukocyte trafficking, macrophage activation and phagocytosis. Also, key hub genes activate the complement cascade and play an important role during these early phases of disease development resulting in smooth muscle cell and collagen deposition abnormalities. The relationship between ITGB2, the complement cascade and atherosclerosis are complex and involves multiple biological pathways and immune cells. Further research is needed to fully understand the role of these mechanistic pathways in the development and progression of atherosclerosis and to identify potential therapeutic targets with the potential to prevent atherosclerosis progression at this stage of disease.

4.4. Study limitations

The present work was limited to whole tissue gene expression analysis instead of single-cell RNA sequencing, which would have provided a more precise tracking of the expression profile of each cell type. Furthermore, the RNA-Seq of pooled samples prevented us from exploring gene expression variability between individuals and correlate it with lesion phenotypes. Additionally, the ITGB2 overexpression

experiment was restricted to porcine aortic endothelial cells (PAECs). Given that endothelial cells are not the predominant cell type in fibrous atheroma, assessing the potential role of ITGB2 in regulating other genes might not adequately mimic the complexity of atherosclerotic disease, especially at the early stages of fibroatheroma. To gain more comprehensive insights into the regulatory mechanisms governing atherosclerosis lesions, it would be valuable to investigate macrophages, myofibroblasts, and aortic smooth muscle cells, as these cell types may exhibit varying responses and mechanistic pathways.

While we attempted to replicate ITGB2 experiments in aortic smooth muscles, our data (not shown) displayed a change in the morphology of these cells to a round shape. Hence, whether ITGB2 overexpression in SMCs results in a phenotypic switch or is a result of a single culture must be investigated. A more suitable approach to studying the role of ITGB2 may involve using a 3D culture or co-culture system to mimic the in vivo cellular environment better.

The present study did not evaluate the presence and type of inflammation markers in the circulation. Nevertheless, our RNA sequencing data revealed significant expression of inflammation-related genes such as Complement C3, C2, C1QA, B, CXCL14, and cytokine receptors like CXCR4 and CSF1R in the WMS-FH lesions. These findings provide substantial evidence supporting the presence of inflammation in the tissue. The identified pathways in this study serve as a robust foundation for our conclusions.

5. Conclusions

In the WMS-FH, the development of fibroatheromas is predominantly driven by cellular and complement-related inflammatory pathways. RNA-Seq results demonstrated unique differential gene expression patterns between abdominal aortic tissue with atherosclerotic lesions (WMS-FH) and lesion-free tissues (WMS normal), at the gene and isoform levels. Ten hub genes were identified as potential therapeutic targets. The manipulation of *ITGB2* expression, the top-ranked hub gene, affected the expression of interconnecting genes. Overall, this study identified key pathways and hub genes associated with atherosclerosis development in WMS-FH. Importantly, we demonstrated that WMS-FH has remarkable similarities to human atherosclerosis at the levels of gene expression and involved pathways allowing the identification of candidate genes with promising therapeutic potential.

Author contributions

JG, JR, AP, KG, and HK: Conceived and designed the study. JG, WS, and AP: performed histopathology and data interpretation. HN: performed the experiments, data analysis and interpretations. DS: participated in data interpretation and revised the manuscript. HN, MS, and CB: participated in bioinformatics analysis. HN wrote and revised the manuscript. All the authors contributed to the manuscript and approved the submitted version.

Financial support

This work was supported by the Cardiovascular Research Foundation, NY, USA.

Data availability

<https://www.ncbi.nlm.nih.gov/geo/query/acc.cgi?acc=GSE199592>.

Declaration of competing interest

The authors declare that they have no known competing financial interests or personal relationships that could have appeared to influence the work reported in this paper.

Acknowledgments

We thank the Swine Research Teaching Center staff for their diligent work in caring for the animals and Nell Bekiares for helping with tissue collection and preservation. We also thank Charles Gersbach for donating the dCas9-p300 and psPgRNA plasmids used in this study.

Appendix A. Supplementary data

Supplementary data to this article can be found online at <https://doi.org/10.1016/j.athplu.2023.11.001>.

References

- [1] Mundi S, Massaro M, Scoditti E, Carluccio MA, van Hinsbergh VWM, Iruela-Arispe ML, de Caterina R. Endothelial permeability, LDL deposition, and cardiovascular risk factors-A review. *Cardiovasc Res* 2018;114:35–52. <https://doi.org/10.1093/cvr/cvx226>.
- [2] Tavares JC, Muscará MN. Adhesion Molecules and Endothelium, Endothelium and Cardiovascular Diseases: Vascular Biology and Clinical Syndromes 2018:189–201. <https://doi.org/10.1016/B978-0-12-812348-5.00014-3>.
- [3] Fuhrman B, Partoush A, Volkova N, Aviram M. Ox-LDL induces monocyte-to-macrophage differentiation in vivo: possible role for the macrophage colony stimulating factor receptor (M-CSF-R). *Atherosclerosis* 2008;196:598–607. <https://doi.org/10.1016/j.atherosclerosis.2007.06.026>.
- [4] Fernando S, Bursill CA, Nicholls SJ, Psaltis PJ. Pathophysiology of atherosclerosis. In: *Mechanisms of vascular disease*. Switzerland: Springer Nature; 2020. p. 19–45. https://doi.org/10.1007/978-3-030-43683-4_2.
- [5] Mohanta SK, Weber C, Yin C, Habenicht AJR. The dawn has come for new therapeutics to treat atherosclerosis: targeting neuroimmune cardiovascular interfaces in artery brain circuits. *Clin Transl Med* 2022;12. <https://doi.org/10.1002/ctm2.1040>.
- [6] Márquez AB, van der Vorst EPC, Maas SL. Key chemokine pathways in atherosclerosis and their therapeutic potential. *J Clin Med* 2021;10. <https://doi.org/10.3390/jcm10173825>.
- [7] Yurdagul A. Crosstalk between macrophages and vascular smooth muscle cells in atherosclerotic plaque stability. *Arterioscler Thromb Vasc Biol* 2022. <https://doi.org/10.1161/ATVBAHA.121.316233>.
- [8] Hetherington I, Totary-Jain H. Anti-atherosclerotic therapies: milestones, challenges, and emerging innovations. *Mol Ther* 2022;30:3106–17. <https://doi.org/10.1016/j.ymthe.2022.08.024>.
- [9] Bäck M, Hansson G. Basic mechanisms of atherosclerosis. In: *Chronic coronary artery disease: a companion to Braunwald's heart disease*. Elsevier Inc; 2018. p. 45–54. <https://doi.org/10.1016/B978-0-323-42880-4.00004-2>.
- [10] Hasler-Rapacz J, Ellegren H, Fridolfsson A, Kirkpatrick B, Kirk S, Andersson L, Rapacz J. Identification of a mutation in the low density lipoprotein receptor gene associated with recessive familial hypercholesterolemia in swine. *Am J Med Genet* 1998. [https://doi.org/10.1002/\(SICI\)1096-8628\(19980413\)76:5<379::AID-AJMG3>3.0.CO;2-I](https://doi.org/10.1002/(SICI)1096-8628(19980413)76:5<379::AID-AJMG3>3.0.CO;2-I).
- [11] Schomberg DT, Tellez A, Meudt JJ, Brady DA, Dillon KN, Arowolo FK, Wicks J, Rousselle SD, Shanmuganayagam D. Miniature swine for preclinical modeling of complexities of human disease for translational scientific discovery and accelerated development of therapies and medical devices. *Toxicol Pathol* 2016;44:299–314. <https://doi.org/10.1177/0192623315618292>.
- [12] Hasler-Rapacz J, Prescott MF, von Linden-Reed J, Rapacz JM, Hu Z, Rapacz J. Elevated concentrations of plasma lipids and apolipoproteins B, C-III, and E are associated with the progression of coronary artery disease in familial hypercholesterolemic swine. *Arterioscler Thromb Vasc Biol* 1995;15:583–92. <https://doi.org/10.1161/01.ATV.15.5.583/FORMAT/EPUB>.
- [13] Schinkel AFL, Krueger CG, Tellez A, Granada JF, Reed JD, Hall A, Zang W, Owens C, Kaluza GL, Staub D, Coll B, ten Cate FJ, Feinstein SB. Contrast-enhanced ultrasound for imaging vasa vasorum: comparison with histopathology in a swine model of atherosclerosis. *Eur J Echocardiogr* 2010;11:659–64. <https://doi.org/10.1093/ejehocardiography/jeq048>.
- [14] Bahlis M, Bidwell CA, Hu J, Krueger CG, Reed JD, Tellez A, Kaluza GL, Granada JF, van Alstine WG, Newcomer SC. Gene expression differences in healthy brachial and femoral arteries of Rapacz familial hypercholesterolemic swine. *Physiol Genom* 2011;43:781–8. <https://doi.org/10.1152/physiolgenomics.00151.2010>.
- [15] Bahlis M, Bidwell CA, Hu J, Tellez A, Kaluza GL, Granada JF, Krueger CG, Reed JD, Laughlin H, van Alstine WG, Newcomer SC. Gene expression differences during the heterogeneous progression of peripheral atherosclerosis in familial hypercholesterolemic swine. 2013. <https://doi.org/10.1186/1471-2164-14-443>.
- [16] Thim T, Hagensen MK, Drouet L, Bal Dit Sollier C, Bonneau M, Granada JF, Nielsen LB, Paaske WP, Botker HE, Falk E. Familial hypercholesterolaemic downsized pig with human-like coronary atherosclerosis: a model for preclinical studies. *EuroIntervention* 2010;6:261–8. [10.4244/EI](https://doi.org/10.4244/EI).
- [17] Tellez A, Krueger CG, Seifert P, Winsor-Hines D, Piedrahita C, Cheng Y, Milewski K, Aboudi MS, Yi G, McGregor JC, Crenshaw T, Reed JD, Huibregtse B, Kaluza GL, Granada JF. Coronary bare metal stent implantation in homozygous LDL receptor deficient swine induces a neointimal formation pattern similar to humans. *Atherosclerosis* 2010;213:518–24. <https://doi.org/10.1016/j.atherosclerosis.2010.09.021>.

- [18] Tellez A, Seifert PS, Donskoy E, Sushkova N, Pennington DE, Milewski K, Krueger CG, Kaluza GL, Eppihimer MJ, Huijbregtse BA, Dawkins KD, Granada JF. Experimental evaluation of efficacy and healing response of everolimus-eluting stents in the familial hypercholesterolemic swine model: a comparative study of bioabsorbable versus durable polymer stent platforms. *Coron Artery Dis* 2014;25: 198–207. <https://doi.org/10.1097/MCA.0000000000000099>.
- [19] Granada JF, Milewski K, Zhao H, Stankus JJ, Tellez A, Aboodi MS, Kaluza GL, Krueger CG, Virmani R, Schwartz LB, Nikanorov A. Vascular response to zotarolimus-coated balloons in injured superficial femoral arteries of the familial hypercholesterolemic swine. *Circ Cardiovasc Interv* 2011;4:447–55. <https://doi.org/10.1161/CIRCINTERVENTIONS.110.960260>.
- [20] NIH Od, Oer Olaw. GUIDE laboratory animals for the care and use of eighth edition committee for the update of the guide for the Care and use of laboratory animals institute for laboratory animal research division on earth and life studies. THE NATIONAL ACADEMIES PRESS; 2011. p. 1–209. <http://www.nap.edu>. [Accessed 26 January 2022].
- [21] Animal Welfare Act as Amended. 7 USC §. 2013. p. 2132–59.
- [22] Langmead B, Salzberg SL. Fast gapped-read alignment with Bowtie 2. *Nat Methods* 2012;9:357–9. <https://doi.org/10.1038/nmeth.1923>.
- [23] Li B, Dewey CN. RSEM: accurate transcript quantification from RNA-Seq data with or without a reference genome. *BMC Bioinf* 2011;12:1–16. <https://doi.org/10.1186/1471-2105-12-323/TABLES/6>.
- [24] Robinson MD, McCarthy DJ, Smyth GK. edgeR: a Bioconductor package for differential expression analysis of digital gene expression data. *Bioinform Appl* 2010;26:139–40. <https://doi.org/10.1093/bioinformatics/btp616>.
- [25] Shen S, Won Park J, Lu Z, Lin L, Henry MD, Nian Wu Y, Zhou Q, Xing Y. rMATS: robust and flexible detection of differential alternative splicing from replicate. *RNA-Seq data* 2022;16. <https://doi.org/10.1073/pnas.1419161111>. n.d.
- [26] Livak KJ, Schmittgen TD. Analysis of relative gene expression data using real-time quantitative PCR and the 2-ΔΔCT method. *Methods* 2001;25:402–8. <https://doi.org/10.1006/meth.2001.1262>.
- [27] Szklarczyk D, Franceschini A, Wyder S, Forslund K, Heller D, Huerta-Cepas J, Simonovic M, Roth A, Santos A, Tsafou KP, Kuhn M, Bork P, Jensen LJ, von Mering C. STRING v10: protein-protein interaction networks, integrated over the tree of life. *Nucleic Acids Res* 2015;43:D447–52. <https://doi.org/10.1093/nar/gku1003>.
- [28] Bindea G, Mlecnik B, Hackl H, Charoentong P, Tosolini M, Kirilovsky A, Fridman W-H, Pagès F, Trajanoski Z, Galon J. ClueGO: a Cytoscape plug-in to decipher functionally grouped gene ontology and pathway annotation networks. *Bioinform Appl* 2009;25:1091–3. <https://doi.org/10.1093/bioinformatics/btp101>.
- [29] Chin CH, Chen SH, Wu HH, Ho CW, Ko MT, Lin CY. cytoHubba: identifying hub objects and sub-networks from complex interactome. *BMC Syst Biol* 2014;8. <https://doi.org/10.1186/1752-0509-8-S4-S11>.
- [30] Haussler M, Schönig K, Eckert H, Eschstruth A, Miané J, Renaud JB, Schneider-Maunoury S, Shkumatava A, Teboul L, Kent J, July JS, Concordet JP. Evaluation of off-target and on-target scoring algorithms and integration into the guide RNA selection tool CRISPOR. *Genome Biol* 2016;17:1–12. <https://doi.org/10.1186/s13059-016-1012-2>.
- [31] Thim T, Hagensen MK, Drouet L, Bal Dit Sollier C, Bonneau M, Granada JF, Nielsen LB, Paaske WP, Bøtker HE, Falk E. Familial hypercholesterolaemic downsized pig with human-like coronary atherosclerosis: a model for preclinical studies. *EuroIntervention* 2010;6:261–8. 10.4244/.
- [32] Tellez A, Seifert PS, Donskoy E, Sushkova N, Pennington DE, Milewski K, Krueger CG, Kaluza GL, Eppihimer MJ, Huijbregtse BA, Dawkins KD, Granada JF. Experimental evaluation of efficacy and healing response of everolimus-eluting stents in the familial hypercholesterolemic swine model: a comparative study of bioabsorbable versus durable polymer stent platforms. *Coron Artery Dis* 2014;25: 198–207. <https://doi.org/10.1097/MCA.0000000000000099>.
- [33] Granada JF, Milewski K, Zhao H, Stankus JJ, Tellez A, Aboodi MS, Kaluza GL, Krueger CG, Virmani R, Schwartz LB, Nikanorov A. Vascular response to zotarolimus-coated balloons in injured superficial femoral arteries of the familial hypercholesterolemic swine. *Circ Cardiovasc Interv* 2011;4:447–55. <https://doi.org/10.1161/CIRCINTERVENTIONS.110.960260>.
- [34] Koskinas KC, Sukhova GK, Baker AB, Papafakis MI, Chatzizisis YS, Coskun AU, Quillard T, Jonas M, Maynard C, Antoniadis AP, Shi GP, Libby P, Edelman ER, Feldman CL, Stone PH. Thin-capped atheromata with reduced collagen content in pigs develop in coronary arterial regions exposed to persistently low endothelial shear stress. *Arterioscler Thromb Vasc Biol* 2013;33:1494–504. <https://doi.org/10.1161/ATVBAHA.112.300827/FORMAT/EPUB>.
- [35] Nadkarni SK, Bouma BE, de Boer J, Tearney GJ. Evaluation of collagen in atherosclerotic plaques: the use of two coherent laser-based imaging methods. *Laser Med Sci* 2009;24:439–45. <https://doi.org/10.1007/s10103-007-0535-x>.
- [36] Nadkarni SK, Pierce MC, Park BH, de Boer JF, Whittaker P, Bouma BE, Bressner JE, Halpern E, Houser SL, Tearney GJ. Measurement of collagen and smooth muscle cell content in atherosclerotic plaques using polarization-sensitive optical coherence tomography. *J Am Coll Cardiol* 2007;49:1474–81. <https://doi.org/10.1016/j.jacc.2006.11.040>.
- [37] Tan X, Zhang X, Pan L, Tian X, Dong P. Identification of key pathways and genes in advanced coronary atherosclerosis using bioinformatics analysis. *BioMed Res Int* 2017;2017:1–12. <https://doi.org/10.1155/2017/4323496>.
- [38] Yang R, Yao L, Du C, Wu Y. Identification of key pathways and core genes involved in atherosclerotic plaque progression. *Ann Transl Med* 2021;9:267. <https://doi.org/10.21037/atm-21-193>. –267.
- [39] Huo T-M, Wang Z-W. Comprehensive analysis to identify key genes involved in advanced atherosclerosis. 2021. <https://doi.org/10.1155/2021/4026604>.
- [40] Schenkel AR, Mamdouh Z, Muller WA. Locomotion of monocytes on endothelium is a critical step during extravasation. 2004 *Nat Immunol* 2004;5(4):393–400. <https://doi.org/10.1038/ni1051>. 5.
- [41] Olson TS, Ley K. Chemokines and chemokine receptors in leukocyte trafficking. *Am J Physiol Regul Integr Comp Physiol* 2002;283:R7–28. <https://doi.org/10.1152/ajpregu.00738.2001>.
- [42] Li Y, Zhu H, Zhang Q, Han X, Zhang Z, Shen L, Wang L, Lui KO, He B, Zhou B. Smooth muscle-derived macrophage-like cells contribute to multiple cell lineages in the atherosclerotic plaque. *Cell Discov* 2021;7. <https://doi.org/10.1038/s41421-021-00328-4>.
- [43] Basatemur GL, Jørgensen HF, Clarke MCH, Bennett MR, Mallat Z. Vascular smooth muscle cells in atherosclerosis. *Nat Rev Cardiol* 2019;16:727–44. <https://doi.org/10.1038/s41569-019-0227-9>.
- [44] Bennett MR, Sinha S, Owens GK. Vascular smooth muscle cells in atherosclerosis. *Circ Res* 2016;118:692–702. <https://doi.org/10.1161/CIRCRESAHA.115.306361>.
- [45] Grootaert MOJ, Moulis M, Roth L, Martinet W, Vindis C, Bennett MR, de Meyer GRY. Vascular smooth muscle cell death, autophagy and senescence in atherosclerosis. *Cardiovasc Res* 2018;114:622–34. <https://doi.org/10.1093/cvr/cvy007>.
- [46] Chinetti-Gbaguidi G, Daoudi M, Rosa M, Vinod M, Louvet L, Copin C, Fanchon M, Vanhoutte J, Derudas B, Belloy L, Haulon S, Zawadzki C, Susen S, Massy ZA, Eeckhoutte J, Staels B. Human alternative macrophages populate calcified areas of atherosclerotic lesions and display impaired RANKL-induced osteoclastic bone resorption activity. *Circ Res* 2017;121:19–30. <https://doi.org/10.1161/CIRCRESAHA.116.310262>.
- [47] Krishnan P, Purushothaman KR, Purushothaman M, Baber U, Tarricone A, Vasquez M, Wiley J, Kini A, Sharma SK, O'Connor WN, Moreno PR. Relation of internal elastic lamellar layer disruption to neointimal cellular proliferation and type III collagen deposition in human peripheral artery stenosis. *Am J Cardiol* 2016;117:1173–9. <https://doi.org/10.1016/j.amjcard.2016.01.006>.
- [48] Adeva-Andany MM, Adeva-Contreras L, Fernández-Fernández C, González-Lucán M, Funcasta-Calderón R. Elastic tissue disruption is a major pathogenic factor to human vascular disease. *Mol Biol Rep* 2021;48:4865–78. <https://doi.org/10.1007/s11033-021-06478-8>.
- [49] Coen M, Gabbiani G, Bochaton-Piallat ML. Myofibroblast-mediated adventitial remodeling: an underestimated player in arterial pathology. *Arterioscler Thromb Vasc Biol* 2011;31:2391–6. <https://doi.org/10.1161/ATVBAHA.111.231548>.
- [50] Galis ZS, Sukhova GK, Lark MW, Libby P. Increased expression of matrix metalloproteinases and matrix degrading activity in vulnerable regions of human atherosclerotic plaques. *J Clin Invest* 1994;94:2493. <https://doi.org/10.1172/JCI117619>.
- [51] Klaus V, Schmies F, Reeps C, Trenner M, Geisbüsch S, Lohoefer F, Eckstein H-H, Pelisek J. Cathepsin S is associated with degradation of collagen I in abdominal aortic aneurysm. *Vasa* 2018;47:285–93. <https://doi.org/10.1024/0301-1526/a000701>.
- [52] Misra A, Rehan R, Lin A, Patel S, Fisher EA. Emerging concepts of vascular cell clonal expansion in atherosclerosis. *Arterioscler Thromb Vasc Biol* 2022;42: E74–84. <https://doi.org/10.1161/ATVBAHA.121.316093>.
- [53] Wang Y, Nanda V, Drenzo D, Ye J, Xiao S, Kojima Y, Howe KL, Jarr K-U, Flores AM, Tsantilis P, Tsao N, Rao A, Newman AAC, v Eberhard A, Priest JR, Ruusalepp A, Pasterkamp G, Maegdefessel L, Miller CL, Lind L, Koplev S, M Björkegren JL, Owens GK, Ingelsson E, Weissman IL, Leeper NJ. Clonally expanding smooth muscle cells promote atherosclerosis by escaping efferocytosis and activating the complement cascade. *Proc Natl Acad Sci USA* 2022;117. <https://doi.org/10.1073/pnas.2006348117/-/DCSupplemental>.
- [54] Wirla RC, Wagh D, Paik DT, Pjanic M, Nguyen T, Miller CL, Kundu R, Nagao M, Collier J, Koyano TK, Fong R, Woo YJ, Liu B, Montgomery SB, Wu JC, Zhu K, Chang R, Alamprese M, Tallquist MD, Kim JB, Quertermous T. Atheroprotective roles of smooth muscle cell phenotypic modulation and the TCF21 disease gene as revealed by single-cell analysis. *Nat Med* 2019;25:1280–9. <https://doi.org/10.1038/s41591-019-0512-5>.
- [55] Ma WF, Hodonsky CJ, Turner AW, Wong D, Song Y, Mosquera JV, Ligay Av, Slenders L, Gancayco C, Pan H, Barrientos NB, Mai D, Alencar GF, Owsiany K, Owens GK, Reilly MP, Li M, Pasterkamp G, Mokry M, van der Laan SW, Khomtchouk BB, Miller CL. Enhanced single-cell RNA-seq workflow reveals coronary artery disease cellular cross-talk and candidate drug targets. *Atherosclerosis* 2022;340:12–22. <https://doi.org/10.1016/j.atherosclerosis.2021.11.025>.
- [56] Xu J, Yang Y. Potential genes and pathways along with immune cells infiltration in the progression of atherosclerosis identified via microarray gene expression dataset re-analysis. *Vascular* 2020;28:643–54. <https://doi.org/10.1177/1708538120922700>.
- [57] Wan Z, Zhao B, Zhang X, Zhao Y. Drug discovery in cardiovascular disease identified by text mining and data analysis. *Ann Cardiothorac Surg* 2020;9: 3089–99. <https://doi.org/10.21037/apm-20-705>.
- [58] Zhao B, Wang D, Liu Y, Zhang X, Wan Z, Wang J, Su T, Duan L, Wang Y, Zhang Y, Zhao Y. Six-gene signature associated with immune cells in the progression of atherosclerosis discovered by comprehensive bioinformatics analyses. *Cardiovasc Ther* 2020;2020. <https://doi.org/10.1155/2020/1230513>.
- [59] Shen Y, rong Xu L, Tang X, po Lin C, Yan D, Xue S, zhe Qian R, qiao Guo D. Identification of potential therapeutic targets for atherosclerosis by analysing the gene signature related to different immune cells and immune regulators in atheromatous plaques. *BMC Med Genom* 2021;14. <https://doi.org/10.1186/s12920-021-00991-2>.

- [60] Meng Y, Zhang C, Liang L, Wei L, Wang H, Zhou F, Li R, Zou D, Huang X, Liu J. Identification of potential key genes involved in the carotid atherosclerosis. *Clin Interv Aging* 2021;16:1071–84. <https://doi.org/10.2147/CIA.S312941>.
- [61] Xu J, Chen C, Yang Y. Identification and validation of candidate gene module along with immune cells infiltration patterns in atherosclerosis progression to plaque rupture via transcriptome analysis. *Front Cardiovasc Med* 2022;9. <https://doi.org/10.3389/fcvm.2022.894879>.
- [62] Meerschaert J, Furie MB. Ligands on endothelium, monocytes and ICAM-1, VCAM-1, and other CD11a/CD18, CD11b/CD18, and VLA-4 on migration across endothelium include the adhesion molecules used by monocytes for. 1995. <http://www.jimmunol.org/content/154/8/4099>.
- [63] Kiss MG, Binder CJ. The multifaceted impact of complement on atherosclerosis. *Atherosclerosis* 2022;351:29–40. <https://doi.org/10.1016/j.atherosclerosis.2022.03.014>.
- [64] Niyonzima N, Rahman J, Kunz N, West EE, Freiwald T, Desai Jv, Merle NS, Gidon A, Sporsheim B, Lionakis MS, Evensen K, Lindberg B, Skagen K, Skjelland M, Singh P, Haug M, Ruseva MM, Kolev M, Bibby J, Marshall O, O'Brien B, Deeks N, Afzali B, Clark RJ, Woodruff TM, Pryor M, Yang Z-H, Remaley AT, Mollnes TE, Hewitt SM, Yan B, Kazemian M, Kiss MG, Binder CJ, Halvorsen B, Espevik T, Kemper C. Mitochondrial C5aR1 activity in macrophages controls IL-1 β production underlying sterile inflammation. *Sci Immunol* 2021;6. <https://doi.org/10.1126/sciimmunol.abf2489>.
- [65] Nageh MF, Sandberg ET, Marotti KR, Lin AH, Melchior EP, Bullard DC, Beaudet AL. Deficiency of inflammatory cell adhesion molecules protects against atherosclerosis in mice. *Arterioscler Thromb Vasc Biol* 1997;17:1517–20. <https://doi.org/10.1161/01.ATV.17.8.1517/FORMAT/EPUB>.
- [66] Bhatia VK, Yun S, Leung V, Grimsditch DC, Benson GM, Botto MB, Boyle JJ, Haskard DO. Complement C1q reduces early atherosclerosis in low-density lipoprotein receptor-deficient mice. *Am J Pathol* 2007;170:416–26. <https://doi.org/10.2353/AJPATH.2007.060406>.
- [67] Speidl WS, Kastl SP, Huber K, Wojta J. Complement in atherosclerosis: friend or foe? *J Thromb Haemostasis* 2011;9:428–40. <https://doi.org/10.1111/J.1538-7836.2010.04172.X>.
- [68] Skoglund C, Wetterö J, Bengtsson T. C1q regulates collagen-dependent production of reactive oxygen species, aggregation and levels of soluble P-selectin in whole blood. *Immunol Lett* 2012;142:28–33. <https://doi.org/10.1016/J.IMLET.2011.11.003>.
- [69] Sasaki S, Nishihira K, Yamashita A, Fujii T, Onoue K, Saito Y, Hatakeyama K, Shibata Y, Asada Y, Ohbayashi C. Involvement of enhanced expression of classical complement C1q in atherosclerosis progression and plaque instability: C1q as an indicator of clinical outcome. *PLoS One* 2022;17:e0262413. <https://doi.org/10.1371/journal.pone.0262413>.
- [70] Micklem KJ, Sim RB. Isolation of complement-fragment-iC3b-binding proteins by affinity chromatography. The identification of p150,95 as an iC3b-binding protein. *Biochem J* 1985;231:233–6. <https://doi.org/10.1042/bj2310233>.
- [71] Buono C, Come CE, Witztum JL, Maguire GF, Connelly PW, Carroll M, Lichtman AH. Influence of C3 deficiency on atherosclerosis. *Circulation* 2002;105:3025–31. <https://doi.org/10.1161/01.CIR.0000019584.04929.83>.
- [72] Wei Y, Zhu M, Corbalán-Campos J, Heyll K, Weber C, Schober A. Regulation of Csf1r and Bcl6 in macrophages mediates the stage-specific effects of MicroRNA-155 on atherosclerosis. *Arterioscler Thromb Vasc Biol* 2015;35:796–803. <https://doi.org/10.1161/ATVBAHA.114.304723>.
- [73] Wang M, Subramanian M, Abramowicz S, Murphy AJ, Gonen A, Witztum J, Welch C, Tabas I, Westertep M, Tall AR. Interleukin-3/granulocyte macrophage colony-stimulating factor receptor promotes stem cell expansion, monocytosis, and atheroma macrophage burden in mice with hematopoietic ApoE deficiency. *Arterioscler Thromb Vasc Biol* 2014;34:976–84. <https://doi.org/10.1161/ATVBAHA.113.303097>.
- [74] Spilsbury K, O'Mara MA, Wu WM, Rowe PB, Symonds G, Takayama Y. Isolation of a novel macrophage-specific gene by differential cDNA analysis. *Blood* 1995;85:1620–9. <http://www.ncbi.nlm.nih.gov/pubmed/7888681>.
- [75] Wittwer J, Marti-Jaun J, Hersberger M. Functional polymorphism in ALOX15 results in increased allele-specific transcription in macrophages through binding of the transcription factor SPI1. *Hum Mutat* 2006;27:78–87. <https://doi.org/10.1002/HUMU.20273>.
- [76] Wang H, Jiang H, Cheng XW. Cathepsin S are involved in human carotid atherosclerotic disease progression, mainly by mediating phagosomes: bioinformatics and in vivo and vitro experiments. *PeerJ* 2022;10:e12846. <https://doi.org/10.7717/peerj.12846>.